The Galaxy Disk in Cosmological ontext
Proceedings IAU Symposium No. 254, 2008
J. Andersen, J. Bland-Hawthorn & B. Nordström, eds.

Turbulence in galactic disks: the role of self-gravity and supernova feedback

Oscar Agertz[1], George Lake[1], Ben Moore[1], Lucio Mayer[1,2], Romain Teyssier[1,3] and Alessandro B. Romeo[4]

[1] Institute for Theoretical Physics, University of Zürich, CH-8057 Zürich, Switzerland
[2] Department of Physics, Institute für Astronomie, ETH Zürich, CH-8093 Zürich, Switzerland
[3] Service d'Astrophysique, CEA/DSM/DAPNIA/SAp, Centre d'Etudes de Saclay, L'orme des Merisiers,91191 Gif-sur-Yvette Cedex, France
[4] Onsala Space Observatory, Chalmers University of Technology, SE-43992 Onsala, Sweden

Abstract. Observations of turbulent velocity dispersions in the HI component of galactic disks show a characteristic floor in galaxies with low star formation rates and within individual galaxies the dispersion profiles decline with radius. We carry out several high resolution adaptive mesh simulations of gaseous disks embedded within dark matter haloes to explore the roles of cooling, star-formation, feedback, shearing motions and baryon fraction in driving turbulent motions. In all simulations the disk slowly cools until gravitational and thermal instabilities give rise to a large population of dense self-gravitating cold clouds that at late times have a mass spectrum similar to observations of giant molecular clouds within Local Group spirals. A multi-phase interstellar medium develops with cold clouds embedded within a warm gaseous phase that forms through shock heating. The diffuse gas is highly turbulent and is driven by cloud-cloud tidal interactions and merging together with swing-amplified shearing motions. At low star-formation rates these processes alone can explain the observed HI velocity dispersion profiles and the characteristic value of $\sim 10\,\mathrm{km\,s^{-1}}$ observed within a wide range of disk galaxies. Supernovae feedback creates a significant hot gaseous phase and is an important driver of turbulence in galaxies with a star-formation rate per unit area $\gtrsim 10^{-3}\,M_\odot\,\mathrm{yr^{-1}\,kpc^{-2}}$, in agreement with observations.

Keywords. galaxies:evolution, ISM:clouds, ISM: kinematics and dynamics, turbulence

1. Introduction

The interstellar medium (ISM) is dominated by irregular/turbulent gas motions (e.g. Larson 1981, Elmegreen & Scalo 2004). HI emission lines in most spiral galaxies have characteristic velocity dispersions of $\sigma \sim 10\,\mathrm{km/s}$ on a scale of a few hundred parsecs, exceeding the values expected from purely thermal effects. The data in Fig. 1, assembled by Dib et al. (2006), also shows a transition to much larger values in active/starbursting galaxies. Recent high resolution observations by Petric & Rupen (2007) of the nearly face on disk galaxy NGC 1058 (see also Dickey et al. 1990) provides us with the currently best data on the radial behavior of the vertical velocity dispersion. They find that the dispersion declines with radius from $\sim 12-15\ \mathrm{km\,s^{-1}}$ in the inner parts to $\sim 4-6\ \mathrm{km\,s^{-1}}$ in the outer and is uncorrelated with active regions such as star formation sites and spiral arms. This is attributed to small scale ($< 0.7\,\mathrm{kpc}$) bulk motions.

The main source(s) of energy driving the ISM turbulence is still not clear (Burkert 2006), even though several plausible candidates exists e.g. large-scale expanding outflows from high-pressure HII regions, stellar winds, supernovae, self-gravity, and the Magneto-Rotational-Instability (MRI). For a discussion of each mechanism, see Mac Low & Klessen (2004) and references therein.

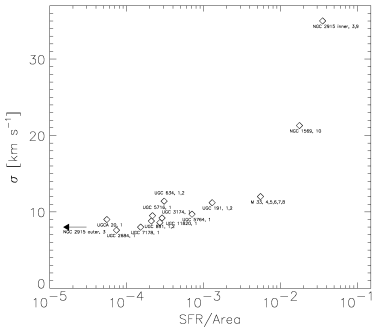

Figure 1. Characteristic velocity dispersions of a sample of galaxies as a function of the derived star formation rate in units of $M_\odot\,\mathrm{yr}^{-1}\,\mathrm{kpc}^{-2}$. References to the observations are given in Dib et al. (2006). Courtesy of Andreas Burkert.

Here, we present the results from high-resolution 3-dimensional Adaptive Mesh Refinement (AMR) simulations set out to form a realistic multi-phase ISM in which we can disentangle the contributing effects of self-gravity and supernovae driven turbulence.

2. Numerical modeling

We use the adaptive mesh refinement (AMR) hydrodynamics code RAMSES (Teyssier 2002 which evolves a gaseous, stellar and dark matter component. The dark matter is here an analytical halo and stars form from the gas above a characteristic density threshold. Our initial condition (IC) is an axisymmetric galactic gas disk in equilibrium with an NFW (Navarro et al. 1997) dark matter halo. The disk is initially isothermal at $T = 10^4$ K having an exponential density profile. We choose to model an M33 type galactic disk as it is a nearby well observed gas rich system. All global characteristics of the initial disk are in agreement with the observations presented by Corbelli (2003) and the gas is assumed to have a mean metallicity of $0.3\,Z_\odot$. We initialize the gas disk in a stable configuration where most of the disk has a gaseous Toomre parameter (Goldreich & Lynden-Bell 1965a) $Q_\mathrm{g} = \kappa c_\mathrm{s}/\pi G\Sigma_\mathrm{g} \sim 2-3$ and expect gravitational instability to occur as the gas undergoes cooling.

We perform a suite of runs set out to investigate the the effects of resolution, cooling floor, supernovae heating and shear. In this proceeding we only discuss the results from our fiducial run, incorporating the modeling described above, and a run with supernovae feedback (see Dubois & Teyssier (2008) for details). We refer to these as RUN1 and RUN3 respectively. Both simulations reach as maximum resolution of $\Delta x \sim 24\,\mathrm{pc}$. A full parameter study is presented in Agertz et al. (in preparation)

3. Results

All simulations evolve in a similar fashion: the initial gas distribution cools down slowly, loses pressure support and contracts in the vertical direction. After a few 100 Myr the central part of the disk is cold enough to become gravitational and thermally unstable and fragments into bound clouds. This process quickly proceeds to larger radii. Non-axis-symmetric instabilities such as swing amplification aids the process everywhere, especially in the outer parts where the gas is only mildly unstable. The formation of bound clouds and elongated structures such as shearing filaments is similar to that found by e.g. Kim & Ostriker (2003) and Kim & Ostriker (2007) for an unstable or marginally

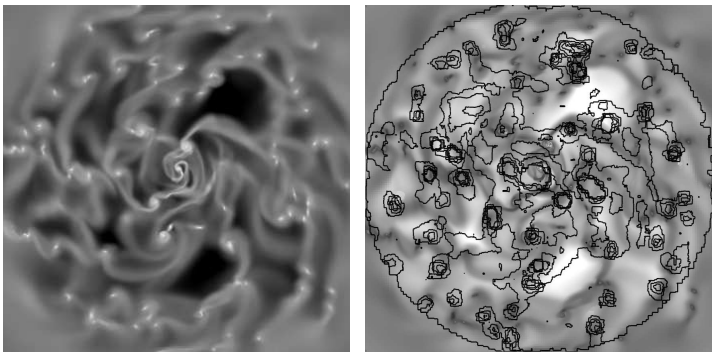

Figure 2. Left: Logarithmic column density plots of the gas in RUN1 at $t = 1.5\,\mathrm{Gyr}$ in the range $\Sigma_\mathrm{g} = 10^{18} - 10^{23}\,\mathrm{cm}^{-3}$. The panel shows a face-on 30×30 kpc map centered on the disk. Right: Inverted density map over-plotted with contours of the effective observable vertical velocity dispersions, $\sigma_{\mathrm{eff},z}$. The contour levels span $2-12\ \mathrm{km\,s}^{-1}$ with a $2\,\mathrm{km\,s}^{-1}$ spacing. Apart from the large velocity dispersion in the central region, well defined peaks of large dispersion exists throughout the disk, sometimes where filaments are interacting. The lack of correlation between the HI and σ-map agrees well with observations.

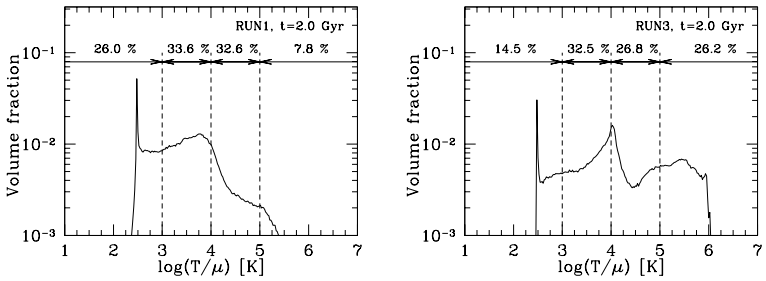

Figure 3. Volume fraction for RUN1 (*left*) and RUN3 (*right*) at $t = 2.0\,\mathrm{Gyr}$. While both models clearly show a cold and warm gas phase, the hot phase only exists when supernova feedback is present.

stable ISM. We observe significant cloud-cloud and cloud-ISM interactions as the disk evolves. The clouds undergo both collisions leading to coalescence as well as tidal and long range interactions inducing torques into the gas. Shearing wavelets form out of the disk in between the cold clouds. These structures interact with each other as well as the clouds for the entire simulation period. In between dense clouds and stretched filaments, the ISM also develops under-dense regions ($\Sigma \lesssim 10^{18}\mathrm{cm}^{-2}$) on scales of 500 pc to several kpc. At later times, signatures of large scale spiral structure appear in the gaseous disk in which the cold clouds align. The left panel of Fig. 2 shows the total gas surface density maps of our fiducial run at $t = 1.5\,\mathrm{Gyr}$. Here, the initially gas and dark matter only system has evolved to a state in which the relative contributions, including the stellar component, and their magnitudes agree well with M33 observations (Corbelli 2003).

A multiphase ISM naturally develops in the simulations as seen from the volume distribution of the gas at the end of the simulation time in Fig. 3. The left panel shows the distribution in RUN1 and we clearly observe a cold and a warm phase while no significant hot phase exists. The warm shock-heated phase is peaking at $T \sim 6\,000 - 8\,000\,\mathrm{K}$. In RUN3, where supernova feedback is allowed, a hot phase is clearly present and the warm gas have now been pushed above the peak of the cooling curve at $T \sim 10^4\,\mathrm{K}$ (see right panel of Fig. 3).

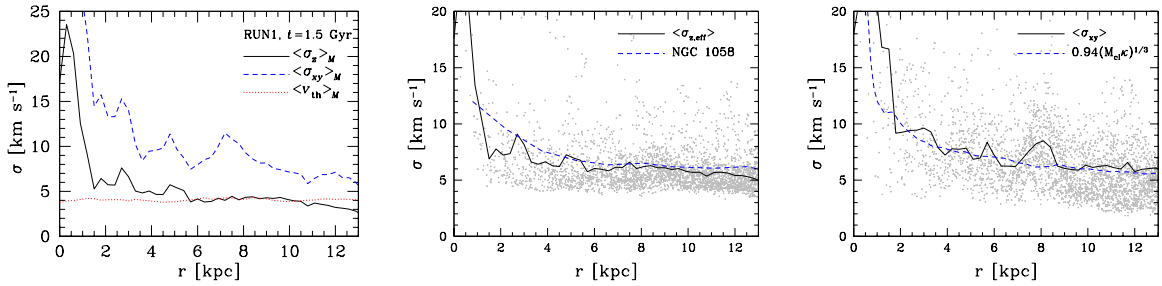

Figure 4. Left: Velocity dispersion components of RUN1. Middle: Comparing the observable vertical velocity dispersion of RUN1 to the observed values of the face-on galaxy NGC 1058. Right: The planar velocity dispersion of RUN1 at $t = 2.0$ Gyr compared to the predicted cloud dispersion from gravitational scattering (see text).

3.1. *Velocity dispersions*

Broadening of spectral lines is mainly due to thermal and Doppler/turbulent effects. We will discuss the thermal effects in terms of the thermal velocity $v_{\rm t} = \sqrt{RT/\mu}$ (i.e. the isothermal sound speed of the gas), where R is the gas constant and μ is the molecular weight. Random bulk motion of the gas is quantified in terms of its turbulent velocity dispersion $\sigma_{\rm t}$. We calculate the net observable dispersion by adding the turbulent and thermal contribution in quadrature, i.e. $\sigma^2_{\rm eff} = v^2_{\rm t} + \sigma^2_t$. In addition, we analyze only the gas that would safely be observed as HI and use the criteria $\rho < 10\,{\rm cm}^{-3}$ (star formation threshold) and $800\,{\rm K} < T < 10\,000\,{\rm K}$.

The left panel in Fig. 4 the radial behaviour of the velocity dispersion for RUN1, where σ_z is the vertical dispersion component and σ_{xy} the planar. σ_z show typical values of $\sim 15\,{\rm km\,s^{-1}}$ in the center and declines to $\sim 3-5\,{\rm km\,s^{-1}}$ at large radii. The velocity dispersion is clearly anisotropic as σ_{xy} is a factor of ~ 2 larger than the vertical dispersion at all times and radii. The shape of the components are tightly correlated at all times suggesting common a origin. The thermal component of the gas lies in the range $4-5\,{\rm km\,s^{-1}}$ in agreement with a warm gas component ($T \sim 1000-2000\,{\rm K}$). By considering a minimal observable, i.e. $\sigma_{\rm eff}$ for the z-component, we clearly find an agreement with observed HI dispersions, i.e. $\sigma_{\rm eff} \sim 12-15\ {\rm km\,s^{-1}}$ in the inner parts declining to $\sim 4-6\ {\rm km\,s^{-1}}$ in the outer. Any inclination would boost these values due to the σ-anisotropy.

We now directly compare our simulations to the HI data of the spiral galaxy NGC 1058 (Dickey et al. 1990 and Petric & Rupen 2007). NGC 1058 is a suitable object for comparisons, as it is comparable in size, surface density and peak rotational velocity to our simulated disk. The galaxy also has a low star formation rate, ${\rm SFR} \sim 3.5\times10^{-2}\,M_\odot\,{\rm yr}^{-1}$ (Ferguson et al. 1998), which places it in the flat part of Fig. 1. Furthermore, by being an almost perfectly face-on galaxy (inclination of $4-11\,^\circ$), we can disentangle the vertical component from the planar. In the middle panel of Fig. 4 we compare $\sigma_{z,{\rm eff}}$ of RUN1 at $t = 1.5\,{\rm Gyr}$ with the observational data of NGC 1058. Our simulation not only reproduces the magnitude of the velocity dispersion but also the declining radial shape.

3.2. *What is the driver of ISM turbulence?*

The driver of the turbulent component of the velocity dispersion is gravity coupled with shear. The galactic disks have, by mass, a wide spectrum of $Q_{\rm g}$ values distributed around a value of marginal stability (e.g. $Q_{\rm g} \sim 0.9$ at $t = 2.0\,{\rm Gyr}$) for a finite thickness disk. The 2D shearing box simulations by Kim & Ostriker (2007) showed that a marginally stable gas disks at $Q_{\rm g} \sim 1.2$ can generate velocity dispersions of the order of the local sound speed, decreasing for larger $Q_{\rm g}$-values (see their Fig. 12). The origin of turbulence

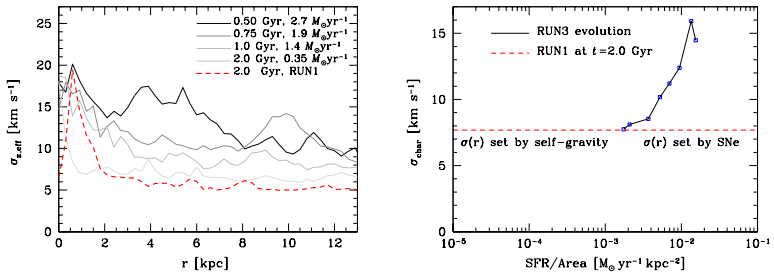

Figure 5. Left: Effect of star formation rate on the observed vertical velocity dispersion in RUN3. The different lines indicate the values at different times and therefore also for different SFRs. There is a clear trend that a lower stellar activity lowers the measured dispersion, approaching the baseline observed dispersion given by RUN1 at $t = 2.0$ Gyr (thick red dashed line). Right: Average velocity dispersion of RUN3 as a function of SFR/Area (black solid line). At late times, and around SFR/Area$\sim 10^{-3}\,M_\odot\,\mathrm{yr}^{-1}\,\mathrm{kpc}^{-2}$, the dispersion is of the same magnitude as in the no-feedback RUN1 (dashed red line).

was here attributed to swing amplification (Goldreich & Lynden-Bell 1965b). Note that the 3D structure of our disks necessitates values $\sim 25\%$ lower for an equivalent stability. As the disks show a wide rangemodeled of Q_g values we will statistically always have a spectrum of swing amplified turbulence across the whole disk for gas that locally behaves in accordance with the simulations of Kim & Ostriker (2007) for $Q_\mathrm{g} > 1.2$.

For small values of Q_g, where the gas has undergone full non-linear gravitational instability, the situation is different. The cold phase dominates the gas mass, even at early times and is therefore locally the most important gravitational source. Direct cloud merging and tidal interactions stirs the inter-cloud medium both radially and vertically. Apart from stirring the gas, the clouds also dissipate energy thermally in shocks which regulates the warm phase of the ISM, forming the $\sim 4-5\,\mathrm{km\,s^{-1}}$ thermal component of σ_eff. Cloud-cloud interaction can be modelled as gravitational scattering and has been studied analytically by e.g. Jog & Ostriker (1988) and Gammie et al. (1991). The semi-analytical perturbation theory model of Gammie et al. (1991) predicts a planar velocity dispersion $\sigma_{xy} \approx 0.94(GM_\mathrm{cl}\kappa)^{1/3}$, where M_cl is a typical mass of a cloud. This relation is derived for a two-dimensional, two-body encounter on radially separated orbits in a shearing disk. However, as these clouds are the main local perturbers by mass we can assume that the diffuse HI gas will approximately be dictated by the cloud ensemble velocities. In the right panel of Fig. 4 we plot σ_{xy} for RUN1 at the end of the simulation and the above equation using a cloud mass $M_\mathrm{cl} \approx 3.5 \times 10^6 M_\odot$, and $\kappa(r)$ of the gas in the simulation. We stress that M_cl is in the high-end of a typical GMC mass spectrum (Blitz 2007). As the clouds in our simulations are submerged in massive HI envelopes, the largest clouds are closer in mass to that of GMC complexes or GMAs (Giant Molecular Associations). The weak dependence on κ can explain why most non star-bursting galaxies seem to plateau at a velocity dispersion between 7 and $11\,\mathrm{km\,s^{-1}}$ (see Fig. 1).

3.3. *Effect of supernova feedback*

Self-gravity driven turbulence may be important for galaxies with a low SFR/Area but cannot be the dominant driver behind the large velocity dispersions correlated with high star formation rates. Observations suggests that galaxies with a SFR/Area $\geqslant$ few $\times$ $10^{-3} M_\odot\,\mathrm{yr}^{-1}\,\mathrm{kpc}^{-2}$ show velocity dispersions of several $10\,\mathrm{km\,s^{-1}}$, see Fig. 1. Dib et al. (2006) showed that strong SN feedback could explain the transition into this range but were unable to explain the other end of the spectrum. In the left panel of Fig. 5 we plot

the effective vertical dispersions for RUN3 at different times and hence different SFRs. The general amplitude of the dispersion declines with SFR and after $t = 1.5$ Gyr (SFR $\approx 0.74\,M_{\odot}\mathrm{yr}^{-1}$) there is little discrepancy between RUN1 and RUN3 suggesting that the effect of SN feedback has saturated. As seen in Fig. 3, more warm gas (close to $\sim 10\,000$ K) exists in RUN3 explaining the $\sim 1\,\mathrm{km\,s}^{-1}$ off-set between RUN1 and RUN3 at large radii. The data shown in Fig. 1 can be reproduced by averaging the velocity dispersion and SFR over a suitable area, hence obtaining a characteristic velocity dispersion $\sigma_{\mathrm{char}}(r)$. Dib et al (2006) used the area $A = \pi(3r_0)^2$, where r_0 is the scale radius of the stellar disk. The right panel of Fig. 5 shows the outcome of this procedure and we clearly detect a supernovae saturation to occur at a SFR/Area of $1 - 2 \times 10^{-3}\,M_{\odot}\,\mathrm{yr}^{-1}\,\mathrm{kpc}^{-2}$, where σ_{char} for RUN1 and RUN3 coincides at $t = 2.0\,\mathrm{Gyr}$. This transition from supernovae to self-gravity induced turbulence can explain why the velocity dispersion of the NGC 1058, having a SFR/Area$\ll 10^{-3}\,M_{\odot}\,\mathrm{yr}^{-1}\,\mathrm{kpc}^{-2}$, is in good agreement with our simulated disk.

4. Conclusion

We have carried out realistic AMR simulations of isolated galactic disks to disentangle the contributing effects of gas self-gravity and supernova feedback to the ISM turbulence. We find that self-gravity driven turbulence dominates the turbulent budget with characteristic HI velocity dispersions of $\sim 10\,\mathrm{km\,s}^{-1}$ as long as the SFR/Area$< 10^{-3}\,M_{\odot}\,\mathrm{yr}^{-1}\,\mathrm{kpc}^{-2}$, Above this values, supernova feedback produces larger velocity dispersions as observed in starbursting/active galaxies (Dib et al. 2006).

References

Blitz L., Fukui Y., Kawamura A., Leroy A., Mizuno N., Rosolowsky E., 2007, in Reipurth B., Jewitt D., Keil K., eds, Protostars and Planets V Giant Molecular Clouds in Local Group Galaxies. pp 81–96

Burkert A., 2006, Comptes Rendus Physique, 7, 433

Corbelli E., 2003, MNRAS, 342, 199

Dib S., Bell E., Burkert A., 2006, ApJ, 638, 797

Dickey J. M., Hanson M. M., Helou G., 1990, ApJ, 352, 522

Dubois Y., Teyssier R., 2008, A&A, 477, 79

Elmegreen B. G., Scalo J., 2004, ARA& A, 42, 211

Ferguson A. M. N., Gallagher J. S., Wyse R. F. G., 1998, AJ, 116, 673

Gammie C. F., Ostriker J. P., Jog C. J., 1991, ApJ, 378, 565

Goldreich P., Lynden-Bell D., 1965a, MNRAS, 130, 97

Goldreich P., Lynden-Bell D., 1965b, MNRAS, 130, 125

Jog C. J., Ostriker J. P., 1988, ApJ, 328, 404

Kim W.-T., Ostriker E. C., 2007, ApJ, 660, 1232

Kim W.-T., Ostriker E. C., Stone J. M., 2003, ApJ, 599, 1157

Larson R. B., 1981, MNRAS, 194, 809

Mac Low M.-M., Klessen R. S., 2004, Reviews of Modern Physics, 76, 125

Navarro J. F., Frenk C. S., White S. D. M., 1997, ApJ, 490, 493

Petric A. O., Rupen M. P., 2007, AJ, 134, 1952

Teyssier R., 2002, A&A, 385, 337